Intuitive Physical Interaction in Macro-Mini Robotic Assistance via a Continuum Parallel Robot

Amir Trabelsi, Arda Yigit, Juan Sandoval, and Sébastien Briot

Abstract Robotic assistants are increasingly used in the operating room to support clinicians during medical procedures, where intuitive and precise physical interaction is essential. However, comanipulation with industrial robots is often limited by their high inertia, resulting in reduced transparency and limited intuitiveness. This paper investigates the concept of using a continuum parallel robot (CPR) in order to create a macro–mini robotic architecture to improve physical human–robot interaction for fast and intuitive pre-positioning of medical tools. The CPR is controlled using a geometrico-static model that allows the user to modify the end-effector equilibrium position through direct physical interaction. Two control strategies are considered: a baseline controller prone to drift, and an interaction-gated controller based on a capacitive touch sensor that regulates the equilibrium in the absence of interaction. Experimental results demonstrate that interaction-gated control eliminates drift while preserving transparency. Disturbance rejection capabilities are further analyzed through stiffness ellipsoids and validated

A. Trabelsi
Nantes Université, École Centrale de Nantes, CNRS, LS2N, UMR 6004, 44321 Nantes, France
e-mail: amir.trabelsi@ls2n.fr

A. Yigit
Nantes Université, École Centrale de Nantes, CNRS, LS2N, UMR 6004, 44321 Nantes, France
e-mail: arda.yigit@ls2n.fr

J. Sandoval
Nantes Université, École Centrale de Nantes, CNRS, LS2N, UMR 6004, 44321 Nantes, France
e-mail: juan.sandoval@ls2n.fr

S. Briot
Nantes Université, École Centrale de Nantes, CNRS, LS2N, UMR 6004, 44321 Nantes, France
e-mail: sebastien.briot@ls2n.fr

experimentally, highlighting the potential of continuum-based macro–mini architectures for intuitive and safe medical robotic assistance.

1 Introduction

The emergence of robotic assistants in the operating room in recent years, dedicated to supporting practitioners in their gestures, has contributed to improved quality of care by increasing precision and reliability, enhancing vigilance, and allowing clinicians to focus primarily on the patient [2]. As a result, extensive research efforts have led to the development and commercialization of robotic assistants for a wide range of medical applications, including orthopedic surgery (e.g., Rosa Knee from Zimmer Biomet), spine surgery (e.g., Mazor X from Medtronic), and urological surgery (e.g., the *da Vinci* Surgical System from Intuitive Surgical).

The effectiveness of such co-manipulated robotic assistants has therefore been well demonstrated. These systems are often based on industrial robots adapted for collaborative operation. However, despite their success, comanipulation with these robots typically relies on classical admittance control strategies. This approach requires practitioners to cope with the high inertia of these systems during manual guidance, which may result in less intuitive interaction than expected. This limitation is particularly critical when the robotic assistant is used as a pre-positioning guide for medical instruments, such as needles or surgical cutters, where fast, precise, and intuitive motions close to the patient are required.

One approach to improve comanipulation intuitiveness consists of favoring low-impedance displacement sensors mounted on the robot structure and mapping the measured sensor motion directly into the robot motion, as proposed in [8]. In the same perspective of decoupling robot dynamics from user motion, macro-mini-robotic architectures, in which a highly dexterous and low-inertia mini robot is mounted on the end-effector of a larger macro robot, have been shown to effectively mitigate the inertia-related limitations of industrial robots during comanipulation tasks. Such approaches have been demonstrated using both passive [7, 3] and active [9] mini systems. While these architectures have been primarily investigated in industrial contexts, their integration into medical robotic systems has strong potential to improve the intuitiveness and responsiveness of physical interaction between practitioners and robotic assistants.

In this work, we explore the concept of using a continuum parallel robot (CPR) in order to create of a macromini robotic architecture for medical assistance, with a particular focus on fast and intuitive pre-positioning of medical tools in the target intervention area. In order to analyze the validity of the concept, a two-degree-of-freedom CPR acting as the mini system is tested as a proof-of-concept. They robot is planned to be mounted later on

(a) (b)

Fig. 1: (a) Working principle of the proposed macro–mini CPR robotic assistant during physical comanipulation by a practitioner, and (b) kinematic scheme of the mini-CPR.

a KUKA LBR iiwa 7 robot serving as the macro robot (Fig. 1(a)), in order to test the feasibility of the approach. The proposed CPR exhibits intrinsic mechanical compliance due to its structure, which enhances safety in the event of unintended contact with the patient or the surrounding medical environment while maintaining extremely low inertia to enable intuitive physical interaction.

Furthermore, the proposed control framework incorporates an external capacitive sensor to distinguish intentional user interaction from system uncertainties and unmodeled disturbances. In addition, a serial passive arm instrumented with encoders and mounted in parallel with the CPR (Fig. 1(b)) provides the current end-effector pose and enables the measurement of the direction and amplitude of the users motion intention, following a noncollocated feedback principle for physical humanrobot interaction with flexible robots, as introduced in [5, 6].

This paper presents the first stage of the analysis of our proof of feasibility of the macro-mini architecture, i.e. the modeling of the compliant mini CPR (Section 2), the proposed control approach (Section 3), and preliminary experimental results demonstrating the system behavior during physical interaction scenarios.

2 Continuum robot modeling

For modeling the CPR, we use the approach proposed in [4]. As depicted in Fig. 1(b), the CPR is made of two flexible rods (Fig. 2). Their proximal extremities are attached to revolute motors at points A_i ($i = 1, 2$) whose axes are directed along $\boldsymbol{z}_0$. Their distal extremities are connected together by the use of a passive revolute joint at point C with an axis parallel to $\boldsymbol{z}_0$. By design, the robot is constrained to stay in the plane $\mathcal{F}_0 : (O\boldsymbol{x}_0\boldsymbol{y}_0)$ thanks to

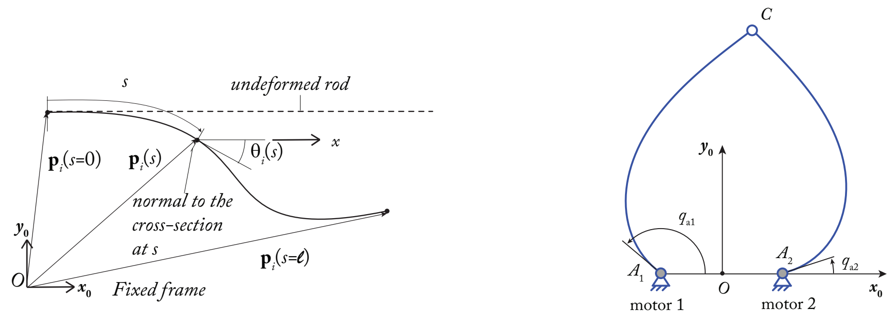

(a) (b)

Fig. 2: (a) Parameterization of the deformation of a slender rod. (b) Kinematic scheme of the CPR.

the presence of a passive rigid and planar RRR serial arm, connected between the base and the revolute joint at point C. Let us denote as $\mathbf{q}_\mathrm{a}$ the vector of the motor positions, containing the orientations θ_{i0} of the first sections of each rod, and as $\mathbf{q}_\mathrm{p}$ the position of the point C in $\mathcal{F}_0$, considered as the robot end-effector coordinates.

The deformations of the flexible rods (Fig. 2(a)) are governed by the Cosserat equations [4], which under the assumptions of planar deformations, neglecting the shear and elongation, as well as the gravity loads, can be written as, for the leg i considered to be straight at rest $(i = 1, 2)$,

$$\begin{cases} \mathbf{p}_i'(s) = \begin{bmatrix} \cos\theta_i(s) \\ \sin\theta_i(s) \end{bmatrix} \\ \theta_i'(s) = \frac{m_{iz}(s)}{EI} \\ \mathbf{n}_i'(s) = \mathbf{0} \\ m_{iz}'(s) = n_{ix}(s)\sin\theta_i(s) - n_{iy}(s)\cos\theta_i(s) \end{cases} \tag{1}$$

where $s \in [0\,\ell]$ is the curvilinear abscissa parameterizing the location of the frame $\mathcal{F}(s) : (S, \boldsymbol{x}(s)\boldsymbol{y}(s))$ with respect to the frame $\mathcal{F}_0$ (Fig. 1(b)), ℓ being the length of the leg i, $\mathbf{p}_i$ is the position of point S in $\mathcal{F}_0$, θ_i the orientation of $\mathcal{F}(s)$ in $\mathcal{F}_0$, $\mathbf{n}_i$ is the force applied on the cross-section at S, with n_{ix} and n_{iy} its components along $\boldsymbol{x}_0$ and $\boldsymbol{y}_0$, and m_{iz} is the moment around $\boldsymbol{z}_0$ on the same cross-section. Additionnally, in these equations, the symbol $(.)'$ denotes the derivative with respect to s, E is the Young's modulus of the material of the rod, and I the second moment of area of the cross-section. Equations (1) can be numerically integrated when knowing the initial conditions $\mathbf{p}_i(s = 0) = \mathbf{p}_{i0}$, $\theta_i(s = 0) = q_{\mathrm{a}i}$, $\mathbf{n}_i(s = 0) = \mathbf{n}_{i0}$, $m_{iz}(s = 0) = m_{iz0}$. Note that an exact solution to (1) exists [1].

Following [4], the geometrico-static model of the CPR is given by:

$$\mathcal{R}(\mathbf{q}_{\rm a}, \mathbf{q}_{\rm p}, \mathbf{q}_{\rm u}) = \begin{bmatrix} \mathbf{n}_1(\ell) + \mathbf{n}_2(\ell) - \mathbf{f}_{ext} \\ m_{1z}(\ell) \\ m_{2z}(\ell) \\ \mathbf{q}_{\rm p} - \mathbf{p}_1(\ell) \\ \mathbf{q}_{\rm p} - \mathbf{p}_2(\ell) \\ \mathbf{e}(\mathbf{q}_{\rm a}, \mathbf{q}_{\rm p}) \end{bmatrix} = \mathbf{0} \tag{2}$$

where $\mathbf{f}_{ext}$ is an external force applied at point C, and $\mathbf{q}_{\rm u} = [\mathbf{n}_{10}^T \ m_{1z0} \ \mathbf{n}_{20}^T \ m_{2z0}]^T$. In these equations, the first line represents the static-force equilibrium at point C, the second and third lines the fact that the passive revolute joint at C cannot transmit any moment. Lines 4 and 5 are the geometric loop-closure constraint equations. Finally, the function $\mathbf{e}(\mathbf{q}_{\rm a}, \mathbf{q}_{\rm p})$ takes the form $\mathbf{e}(\mathbf{q}_{\rm a}, \mathbf{q}_{\rm p}) = \mathbf{q}_{\rm a} - \mathbf{q}_{\rm a}^*$ for solving the forward problem, where $\mathbf{q}_{\rm a}^*$ is the desired value of the motors positions, or the form $\mathbf{e}(\mathbf{q}_{\rm a}, \mathbf{q}_{\rm p}) = \mathbf{q}_{\rm p} - \mathbf{q}_{\rm p}^*$ for solving the inverse problem, where $\mathbf{q}_{\rm p}^*$ is the desired value of the end-effector position. The solutions vanishing the residual $\mathcal{R}$, which is a system of 10 equations for 10 unknowns $(\mathbf{q}_{\rm a}, \mathbf{q}_{\rm p}, \mathbf{q}_{\rm u})$, can be found by using standard root-finding techniques (e.g., Newton-Raphson or Levenberg-Marquardt algorithms).

3 Continuum robot control

The actuators of the parallel continuum robot are considered to be position-controlled. The desired actuator configurations are noted $\mathbf{q}_{\rm a}^*$. Let $\mathbf{q}_{\rm p}^*$ denote the desired end-effector position in the absence of external disturbances. Then, $\mathbf{q}_{\rm p}^*$ and $\mathbf{q}_{\rm a}^*$ are related by the inverse geometrico-static problem (*IGSP*) presented in the previous section, such that $\mathbf{q}_{\rm a}^* = IGSP(\mathbf{q}_{\rm p}^*)$. Furthermore, it is considered that the measurement of the end-effector position $\mathbf{q}_{\rm p}$ is available, which is achieved by instrumenting the passive joints of the planar RRR arm (Fig. 1(b)).

The goal is to design a control strategy that allows the user to modify the equilibrium position of the end-effector through physical interaction, that is, by directly changing the actual end-effector position $\mathbf{q}_{\rm p}$.

Two control modes are considered in this work. **Mode I**, referred to as the *always-active control mode*, is continuously active regardless of whether the operator is interacting with the end-effector. **Mode II**, referred to as the *interaction-gated mode*, is activated when physical interaction with the end-effector is detected to be absent. Interaction detection is achieved using a contact sensor mounted at the end-effector.

In Mode I, the desired end-effector position is defined as the measured actual position: $\mathbf{q}_{\rm p}^* = \mathbf{q}_{\rm p}$. This control mode favors seamless interaction by canceling the restoring forces induced by the elastic deformations of the beams. To achieve this behavior, the actuator positions are continuously updated during end-effector motion so as to compensate for the interaction forces ex-

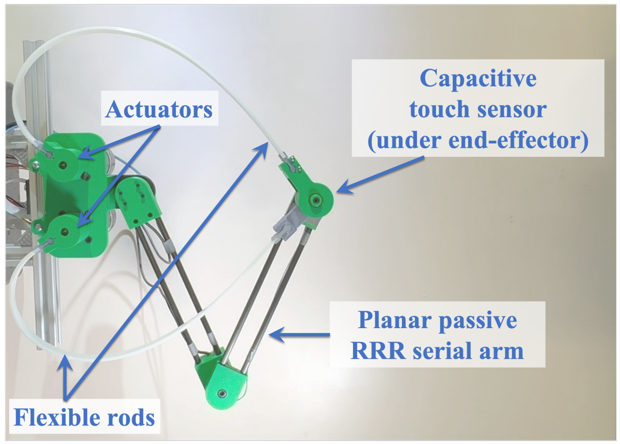

Fig. 3: Experimental setup of the proposed mini-CPR.

perienced by the user. However, when the user is no longer interacting with the end-effector, this mode may lead to drift caused by small external disturbances or discrepancies between the geometrico-static model and the actual robot behavior. To mitigate this drift, Mode II freezes the desired end-effector position $\mathbf{q}_\mathrm{p}^*$ once interaction is no longer detected. As a result, the actuator positions remain constant, and the robot passively rejects external disturbances through its intrinsic mechanical stiffness, allowing the end-effector to remain stable around the last equilibrium configuration.

4 Experimental results

Figure 3 presents the experimental setup used for all tests. The flexible rods are 40-cm long and were fabricated using 3D-printed TPU with a nominal Young's modulus of approximately 50 MPa. Each rod has a rectangular cross section of 10 mm x 3 mm, yielding a second moment of inertia of $2.73e-10$ m^4. The rods are connected at the end-effector through a revolute joint. The base angles of the rods are actuated by two Maxon EC45 Flat 70 W brushless motors, each equipped with high-resolution incremental encoders providing 2028 counts per revolution. The motor axes are spaced 6 cm apart. EPOS 4 drivers provide a velocity-control mode, while a position controller running at 1 kHz computes the desired motor velocities from the desired motor angles. A capacitive touch sensor is mounted at the end-effector to detect contact with the operator. In addition, a passive planar RRR arm connects the base to the end-effector and is instrumented with two optical encoders providing 500 counts per revolution, enabling measurement of the end-effector position.

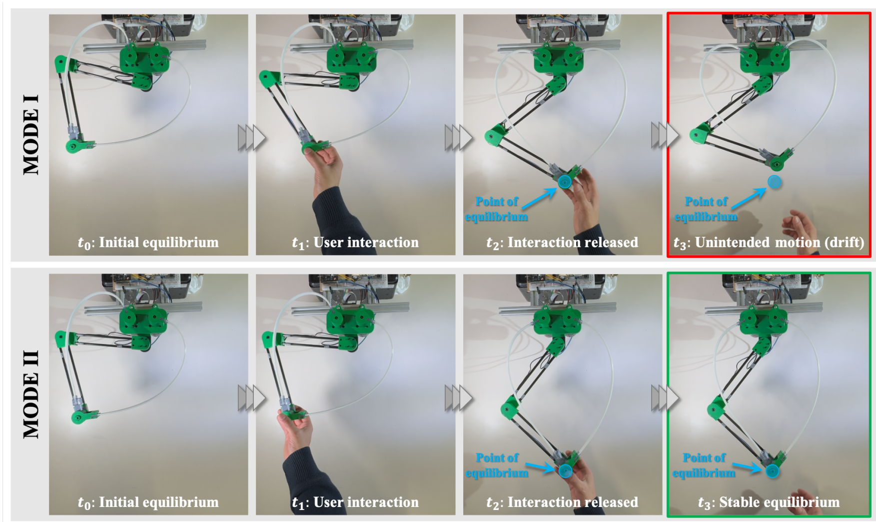

Fig. 4: Comparison of end-effector behavior after interaction release for Mode I and Mode II, showing drift versus stable equilibrium.

The two control modes described in Section 3 were evaluated through physical interaction experiments. These experiments illustrate the behavior of the robot with and without interaction gating. When the contact sensor is not enabled (Mode I), a drift of the end-effector is observed after the operator releases the robot, which is attributed to small modeling inaccuracies and unmodeled disturbances. In contrast, when interaction detection is enabled (Mode II), the robot converges to and remains at the desired equilibrium position without drift. Figure 4 presents a sequence of snapshots illustrating the evolution of the robot behavior in both cases. In addition, a short video accompanying this paper (`https://youtu.be/O_JtGEYN-d4`) provides a qualitative illustration of the experimental results.

To further characterize the mechanical behavior underlying these observations, the stiffness properties of the CPR are analyzed. The stiffness ellipsoid plotted in Fig. 5 is obtained numerically from the 2Œ2 translational stiffness matrix at the shown end-effector position. The translational stiffness matrix $\frac{\partial \mathbf{f}_{ext}}{\partial \mathbf{q}_{\mathrm{p}}}$ is obtained from the linearized geometrico-static model [4]. The stiffness ellipsoid suggests how the robot resists external forces applied at the end-effector in different directions. At the shown end-effector position, the robot is stiffer in the y-direction than in the x-direction, as indicated by the elongated shape of the ellipsoid along the x-axis. This result is validated experimentally in the disturbance-rejection tests shown in Fig. 6: a disturbance is rejected more effectively along the stiffer direction (y-axis) than along the more compliant direction (x-axis).

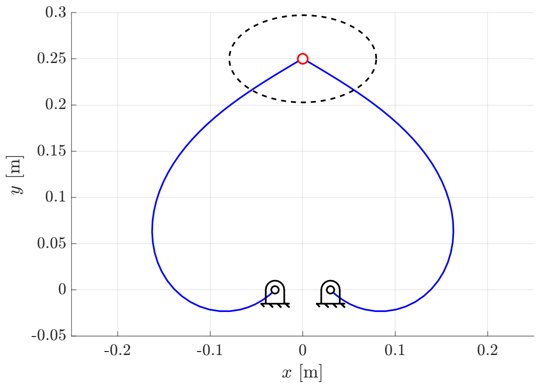

Fig. 5: CPR stiffness ellipsoid at end-effector position $x = 0m$, $y = 0.25m$.

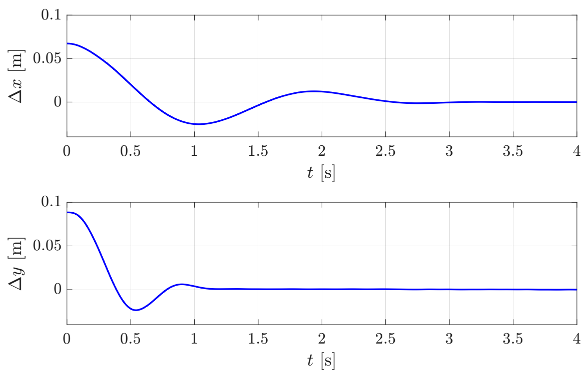

Fig. 6: Disturbance rejection experiments along x and y axes around end-effector position $x = 0m$, $y = 0.25m$.

5 Conclusions

The proposed continuum parallel mini-robot enables high transparency during physical interaction, thanks to the elasticity of the flexible rods, which decouples the actuator inertia from that of the end-effector. Integrated into a macro–mini robotic architecture, this system constitutes a promising low-impedance guidance mechanism for intuitive comanipulation in medical applications.

By introducing actuation into the guidance mechanism, gravity compensation becomes possible, allowing the use of spatial macro-robots while preserving intuitive interaction. A current limitation of the proposed approach lies in the trade-off between interaction transparency and disturbance rejection. Future work will therefore focus on active stiffness modulation strategies to improve robustness against external perturbations, but also on mounting the CPR on the macro robot.

Acknowledgements This project is supported by the French government under the France 2030 Investment Plan, by the Pays de la Loire Region, and by NExT.

References

1. Altuzarra, O., Caballero, D., Campa, F., Pinto, C.: Position analysis in planar parallel continuum mechanisms. Mechanism and Machine Theory **132**, 13–29 (2019)
2. Atchabahian, A., Hemmerling, T.M.: Robotic anesthesia: How is it going to change our practice? Anesthesia and Pain Medicine **4**(1), e16,468 (2014)
3. Badeau, N., Gosselin, C., Foucault, S., Laliberté, T., Abdallah, M.E.: Intuitive physical human-robot interaction: Using a passive parallel mechanism. IEEE Robotics and Automation Magazine **25**(2), 28–38 (2018)
4. Black, C., Till, J., Rucker, D.: Parallel continuum robots: Modeling, analysis, and actuation-based force sensing. IEEE Transactions on Robotics **34**(1), 29–47 (2017)
5. Garant, X., Gosselin, C.: Noncollocated proprioceptive sensing for lightweight flexible robotic manipulators. IEEE/ASME Transactions on Mechatronics **28**(6), 3272–3283 (2023)
6. Garant, X., Gosselin, C.: Whole-body intuitive physical human-robot interaction with flexible robots using non-collocated proprioceptive sensing. IEEE Robotics and Automation Letters **9**(3), 2112–2119 (2024)
7. Labrecque, P.D., Haché, J.M., Abdallah, M., Gosselin, C.: Low-impedance physical human-robot interaction using an activepassive dynamics decoupling. IEEE Robotics and Automation Letters **1**(2), 938–945 (2016)
8. Laliberté, T., Gosselin, C.: Low-impedance displacement sensors for intuitive physical humanrobot interaction: Motion guidance, design, and prototyping. IEEE Transactions on Robotics **38**(3), 1518–1530 (2022)
9. Nguyen, T.S., Campeau-Lecours, A., Gosselin, C.: Physical humanrobot interaction using a macromini robotic system. IEEE/ASME Transactions on Mechatronics **28**(6), 3398–3409 (2023)